

Article

# Ruthenium (Ru) Doped Titanium Dioxide (P25) Electrode for Dye Sensitized Solar Cells

Tharmakularasa Rajaramanan <sup>1,2,3</sup>, Muthukumarasamy Natarajan <sup>4</sup>,  
Punniamoorthy Ravirajan <sup>2</sup> , Meena Senthilnathanan <sup>3,\*</sup> and Dhayalan Velauthapillai <sup>1,\*</sup> 

<sup>1</sup> Faculty of Engineering and Science, Western Norway University of Applied Sciences, P.O. Box 7030, 5020 Bergen, Norway; rramanan9@gmail.com

<sup>2</sup> Clean Energy Research Laboratory, Department of Physics, University of Jaffna, Jaffna 40000, Sri Lanka; pravirajan@univ.jfn.ac.lk

<sup>3</sup> Department of Chemistry, University of Jaffna, Jaffna 40000, Sri Lanka

<sup>4</sup> Department of Physics, Coimbatore Institute of Technology, Coimbatore, Tamil Nadu 641014, India; vishnukutty2002@yahoo.co.in

\* Correspondence: meena@univ.jfn.ac.lk (M.S.); Dhayalan.Velauthapillai@hvl.no (D.V.);  
Tel.: +94-77-714-6469 (M.S.); +47-5558-7711 (D.V.)

Received: 28 February 2020; Accepted: 22 March 2020; Published: 25 March 2020



**Abstract:** In this study, P25-titanium dioxide (TiO<sub>2</sub>) was doped with ruthenium (Ru) by systematically varying the Ru content at 0.15, 0.30, 0.45 and 0.6 mol%. The synthesized Ru-doped TiO<sub>2</sub> nanomaterials have been characterized by X-ray diffraction (XRD), Raman spectroscopy, energy-dispersive X-ray (EDX) analysis, UV-visible (UV-Vis) spectroscopy, and electrochemical impedance (EIS) spectroscopy. The XRD patterns of undoped and Ru-doped TiO<sub>2</sub> nanomaterials confirm the presence of mixed anatase and rutile phases of TiO<sub>2</sub> while EDX spectrum confirms the presence of Ti, O and Ru. Further, UV-visible absorption spectra of doped TiO<sub>2</sub> nanomaterial reveal a slight red shift on Ru-doping. The short circuit current density (J<sub>SC</sub>) of the cells fabricated using the Ru-doped TiO<sub>2</sub> photoanode was found to be dependent on the amount of Ru present in TiO<sub>2</sub>. Optimized cells with 0.3 mol% Ru-doped TiO<sub>2</sub> electrodes showed efficiency which is 20% more than the efficiency of the control cell ( $\eta = 5.8\%$ ) under stimulated illumination (100 mWcm<sup>-2</sup>, 1 sun) with AM 1.5 filter. The increase in J<sub>SC</sub> resulted from the reduced rate of recombination upon doping of Ru and this was confirmed by EIS analysis.

**Keywords:** dye sensitized solar cells; Ru-doped TiO<sub>2</sub>; P25-TiO<sub>2</sub>

## 1. Introduction

Dye-sensitized solar cells (DSSCs) have been studied intensively as an alternative energy source due to their low cost, easy fabrication and more environmentally friendly nature. A DSSC consists of an electron transporting mesoporous metal oxide layer on a transparent conducting oxide coated glass, dye, electrolyte and a counter electrode. Generally, the visible light is converted into electricity in DSSCs through spectral sensitization of wide bandgap semiconductors such as SnO<sub>2</sub> [1], SrTiO<sub>3</sub> [2], Nb<sub>2</sub>O<sub>5</sub> [3], ZnO [4] and TiO<sub>2</sub> [5]. Among the semiconductors explored for DSSCs so far, TiO<sub>2</sub> remains the most promising material [1]. Although natural dyes used as sensitizers in DSSC are cheap compared to synthetic dyes, their reported efficiencies are rather low [6–9]. The concept of a dye-sensitized solid-state solar cell was first proposed by Tennakone et al. in 1988 [10] and then O'Regan and Grätzel reported an efficiency of 7.1% and a current density greater than 12 mAcm<sup>-2</sup> for DSSC in which I<sup>-</sup>/I<sub>3</sub><sup>-</sup> redox couple and TiO<sub>2</sub> were used as liquid electrolyte and ETM, respectively [5]; later, the maximum efficiency of 11.1% was reported by Nazeeruddin et al. [11,12]. However, relaxation of oxidized dye

and recombination processes connected to the charge carriers hinder the performance of DSSCs. One of the alternative strategies to reduce the above said problem in DSSCs is the use of doped TiO<sub>2</sub> electrode. It is evident that dopant materials narrow the bandgap and increase the charge traps of TiO<sub>2</sub> and hence modify the properties, such as conduction band energy, charge transport, recombination and collection of charge carriers [13]. Different dopants, such as transition metals, alkali earth metals [14,15], non-metals [16,17], and rare earth elements [14,18], have been employed; but the incorporation of transition metals into TiO<sub>2</sub> gives rise to the formation of a wide range of new energy levels arising from the partially filled d-orbitals of transition metals close to the conduction band (CB) of TiO<sub>2</sub>, that leads to a reduction in the bandgap and enhancement in harvesting visible light. This makes transition metals suitable for tuning the CB structure [13].

Various transition metals (Ag [19,20], Co [21], Mn [21], Zn [22], Cr [23], Nb [24], W [25], Cu [26], Y [27] and Sc [28]) have been used as dopant in TiO<sub>2</sub>. Ruthenium (Ru) appears to be a good dopant as the Ru<sup>4+</sup> ion has an ionic radius of 0.062 nm which is comparable to that of Ti<sup>4+</sup> ion (0.061 nm) [29]. The utilization of Ru-doped TiO<sub>2</sub> as ETM in DSSCs has not yet been studied in depth. In 2009, Houskova et al. reported that Ru-doping decreases the bandgap of TiO<sub>2</sub> [30], while a contradictory observation was reported by Kong et al. in 2015 [31]. In another study, So and co-workers (2012) reported  $\eta$  of 5.2% using 0.02 at.% Ru-doped TiO<sub>2</sub> nanotube layers in DSSC [32]. Lu et al. (2016) achieved  $\eta$  of 5.39% for the Ru-doped TiO<sub>2</sub> [33]. However, the use of Ru-doped P25-TiO<sub>2</sub> (Degussa P25—commercially purchased TiO<sub>2</sub> nanopowder) as a mesoporous metal oxide in DSSCs has not been reported so far, although Ru-doped P25-TiO<sub>2</sub> has been widely employed to enhance photocatalytic activities [34–36].

In this study, RuCl<sub>3</sub>·xH<sub>2</sub>O was used as a precursor to synthesize Ru-doped electrodes and their performances in DSSCs were investigated by systematically varying the Ru content. The synthesised Ru-doped TiO<sub>2</sub> was characterized by XRD, Raman, UV-visible, EDX and EIS spectroscopy studies.

## 2. Materials and Methods

### 2.1. Materials

All reagents and solvents used were obtained from commercial sources; absolute ethanol (>99%, Sigma Aldrich), Triton TM X-100 (laboratory grade, Sigma-Aldrich), ruthenium (III) chloride hydrate (Reagent Plus-grade, Sigma-Aldrich), titanium dioxide nanopowder (21 nm primary particle size,  $\geq 99.5\%$  trace metals basis, Sigma-Aldrich), di-tetrabutylammonium cis-bis(isothiocyanato)bis(2,2'-bipyridyl-4,4'-dicarboxylato)ruthenium(II) dye (95%, Sigma-Aldrich), acetonitrile (Gradient grade, Sigma-Aldrich), tert-butyl alcohol ( $\geq 99.7\%$ , Sigma-Aldrich), acetylacetone ( $\geq 99.5\%$ , Fluka Analytical).

### 2.2. Methods

#### 2.2.1. Preparation of Ru-Doped TiO<sub>2</sub> Nanomaterials

To achieve a reproducible outcome and comparison, a simple doping of Ru in P25-TiO<sub>2</sub> was used to prepare Ru-doped TiO<sub>2</sub> nanomaterials. Then 0.15, 0.3, 0.45 and 0.6 mol% of RuCl<sub>3</sub>·xH<sub>2</sub>O were added to the TiO<sub>2</sub> nanopowder (P25) and stirred vigorously for one hour at room temperature (step 1, 2) and then it was dried at 100 °C with continuous stirring for 2 hours (step 3). The product was ground well (step 4) and the resulting Ru-TiO<sub>2</sub> powder mixtures were annealed at 500 °C for 3 h (step 5) (Figure 1) [26,35,37,38].

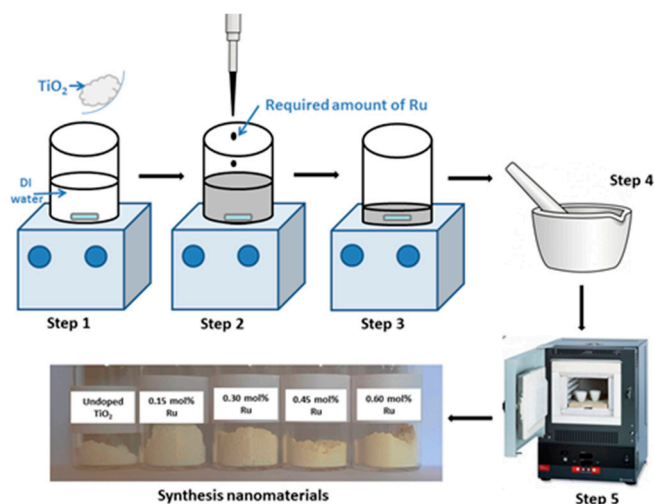


**Figure 1.** Schematic diagram of the synthesis of Ru-doped TiO<sub>2</sub> nanomaterial.

### 2.2.2. Fabrication of DSSCs

The fluorine-doped tin oxide (FTO) coated conducting glass (sheet resistance 7.5 Ω/cm<sup>2</sup>) was used as the current collector. It was cleaned initially with soap water and subsequently with distilled water and ethanol using an ultrasonic bath. Then, the synthesized Ru-doped TiO<sub>2</sub> nanomaterial was made into paste by mixing with deionized water, acetylacetone and Triton TM X-100 binder and coated on FTO by the doctor-blade technique using a glass rod with adhesive tapes (3 M Scotch tapes) as spacers and the thickness of the TiO<sub>2</sub> film was about 7 μm. The prepared Ru-doped TiO<sub>2</sub> films were dried and calcinated at 500 °C for 30 minutes. Then the coated glasses were soaked in 0.3 mM solution of N719 dye in acetonitrile/tert-butyl alcohol (50%v/v) for 12 h. After the dye-sensitization process, the photoanode was washed with acetonitrile to remove the unanchored dye molecules and dried. A platinum-coated FTO glass plate was used as the counter electrode. The dye-coated Ru-doped TiO<sub>2</sub> electrode and Pt counter electrode [26] were used to assemble the cell and I<sup>-</sup>/I<sub>3</sub><sup>-</sup> electrolyte was used as redox electrolyte.

### 2.2.3. Characterization

The structural properties of the synthesized nanomaterials were studied by the X-ray diffraction method using scan range (2θ) between 20° and 95° with step size of 0.02° and scan speed of 1°/min. A Raman spectroscopic study was carried out using a laser confocal Raman microscope (Renishaw, UK, Model: Invia). The optical absorbance spectra were recorded using Shimadzu 1800 Scanning Double Beam UV-visible spectrophotometer. The elemental composition of the synthesized nanomaterials was analyzed by the energy-dispersive X-ray spectroscopy technique. The photovoltaic performance of the cells was studied using Keithley-2400 source measurement unit (SMU) under simulated irradiation of intensity 100 mWcm<sup>-2</sup> with AM 1.5 filter (Pecell-PEC-L12, Japan). Current–voltage (I–V) characteristics in the dark were measured before and after the illumination which confirmed no change in device behaviour [39,40]. The effective area of the photoelectrode was 0.25 cm<sup>2</sup>. Electrochemical impedance spectroscopy (EIS) measurements were carried out on the DSSCs using Metrohm Autolab potentiostat/galvanostat (PGSTAT 128N) with a frequency response analyzer (FRA 32M).

## 3. Results and Discussion

### 3.1. X-ray Siffraction and Raman Spectroscopy

The crystal structure of the synthesized nanomaterials was investigated by the X-ray diffraction method (XRD). Figure 2 represents the XRD patterns of undoped TiO<sub>2</sub> electrode, 0.15, 0.3, 0.45 and 0.6 mol% Ru-doped TiO<sub>2</sub> electrodes and diffraction peaks for 2θ diffraction angles were monitored

between 20° and 80°. The major peaks are observed at 25.2°, 37.6°, 48.2°, 53.7°, 55°, 62.5°, 68.5°, 70.2° and 74.89° and they correspond to the reflection planes of (101), (004), (200), (105), (211), (204), (116), (220) and (215) which confirms the presence of well-crystallized pure anatase TiO<sub>2</sub> phase and peaks at 27.39°, 36.07° and 41.2° correspond to the reflection planes of (110), (101) and (111) for minor rutile TiO<sub>2</sub> phase. This indicates that the anatase and rutile crystal structures are retained even after the TiO<sub>2</sub> being doped with Ru. The average crystallite size was calculated by the Scherrer Equation [15]

$$d = \frac{k\lambda}{B\cos\theta} \quad (1)$$

where  $d$  is the crystallite size,  $k$  is a dimensionless shape factor which has a typical value of about 0.89,  $\lambda$  is the X-ray wavelength of Cu (0.5406 nm),  $\theta$  is the Bragg angle corresponding to the anatase (101) peak, and  $B$  is the line broadening at half the maximum intensity (FWHM). The average crystallite size of undoped TiO<sub>2</sub>, 0.15, 0.3, 0.45 and 0.6 mol% Ru-doped TiO<sub>2</sub> nanomaterials were 17.34, 17.34, 17.79, 17.56 and 17.34 nm and no significant change was observed in the crystallite size. Phase transformation from anatase to rutile was not observed on Ru-doping and hence the crystallite size remains the same. Ismael et al. reported that doping of Ru into the TiO<sub>2</sub> lattice does not change the TiO<sub>2</sub> crystal structure but the predominant anatase peaks of Ru-doped TiO<sub>2</sub> are shifted slightly towards lower  $2\theta$  values when the ruthenium dopant is incorporated in TiO<sub>2</sub> lattice [41]. Ionic radii of Ru<sup>4+</sup> and Ti<sup>4+</sup> are 0.062 and 0.061 nm, respectively. As both the ions have almost the same ionic radii, in the Ru-doped TiO<sub>2</sub>, the incorporated ruthenium ions may be substituting for titanium ions in the lattice. However, crystallite peaks of Ru could not be clearly observed in Ru-doped TiO<sub>2</sub> which may be due to low mol% of the dopant and similar observations have been reported by Senthilnathan et al. (2010) and Elezović et al. (2013) [35,42].

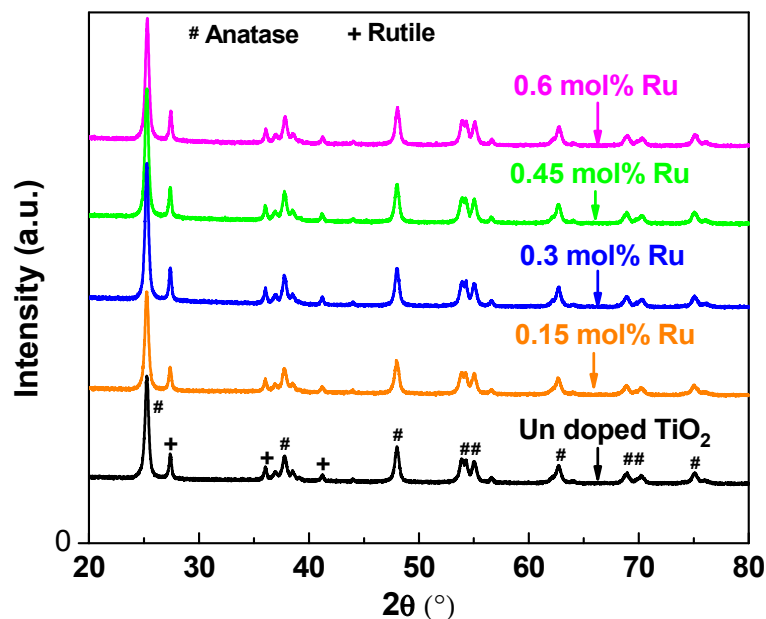
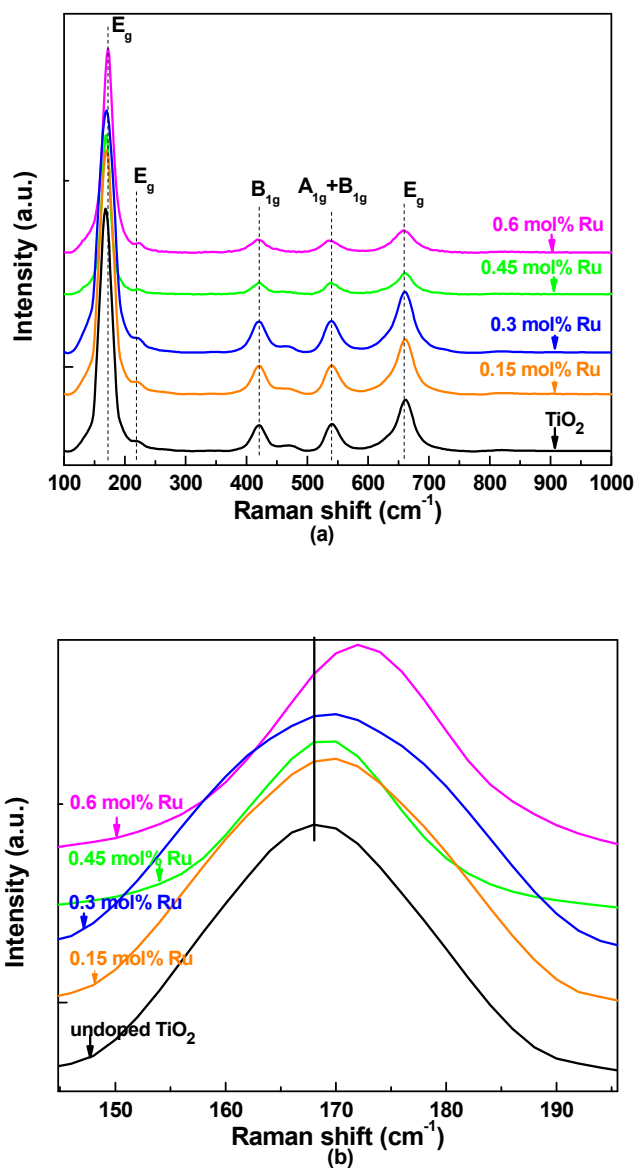


Figure 2. XRD patterns of undoped TiO<sub>2</sub>, 0.15, 0.3, 0.45 and 0.6 mol% Ru-doped TiO<sub>2</sub> nanomaterials.

Figure 3a shows the Raman spectra obtained for the undoped TiO<sub>2</sub> and Ru-doped TiO<sub>2</sub> nanomaterials. The Raman spectrum of the undoped TiO<sub>2</sub> nanoparticles was dominated with five bands corresponding to the six Raman active modes. Well resolved TiO<sub>2</sub> Raman peaks with the D<sub>4h</sub> space group at about 170, 216, and 657 cm<sup>-1</sup> (E<sub>g</sub>), 539 cm<sup>-1</sup> (A<sub>1g</sub> + B<sub>1g</sub>), and 420 cm<sup>-1</sup> (B<sub>1g</sub>) were observed which correspond to the anatase phase of TiO<sub>2</sub> [43]. Figure 3b shows that the peak intensity became weak and also the peak became broader with the increase in the percentage of Ru-doping. In general, the Raman line shape, intensity and position are strongly influenced by lattice strain, defects,

and the crystallite size and shape. There was no peak for the Ru and the same behaviour is observed in the XRD studies. This suggests that Ru ions have been successfully incorporated in the TiO<sub>2</sub> lattice.



**Figure 3.** (a) Raman spectra of undoped TiO<sub>2</sub>, 0.15, 0.3, 0.45 and 0.6 mol% Ru-doped TiO<sub>2</sub> nanomaterials; (b) Detailed E<sub>g</sub>-170 cm<sup>-1</sup> Raman peaks of undoped TiO<sub>2</sub> and Ru-doped TiO<sub>2</sub> nanomaterials.

### 3.2. UV-Visible Absorption Spectroscopy

UV-visible spectroscopy was employed to study the optical properties of the prepared nanomaterials. Five milligrams of the nanomaterial was dispersed in 100 ml of the deionized water in an ultrasonic bath and 1 ml of the dispersed sample was transferred to a standard quartz cuvette for measurement [23]. Figure 4a represents the optical absorption spectra of undoped TiO<sub>2</sub>, 0.15, 0.3, 0.45 and 0.6 mol% Ru-doped TiO<sub>2</sub> nanomaterials. As can be seen from Figure 4a the absorption peak of undoped TiO<sub>2</sub> nanomaterial appears in the UV region whereas there is a slight red shift in the absorption spectrum of Ru-doped TiO<sub>2</sub> and this red shift is found to increase with the increase in Ru-doping indicating the bandgap narrowing due to the introduction of a mid-bandgap or impurity levels located between the valence band and the conduction band of TiO<sub>2</sub>. In addition, the light absorption in the range from 400 to 700 nm is found to increase with increasing Ru content in the Ru-doped TiO<sub>2</sub>, accompanied with a change in the colour from white to reddish black [41].

The bandgap ( $E_g$ ) of undoped  $\text{TiO}_2$ , 0.15, 0.3, 0.45 and 0.6 mol% Ru-doped  $\text{TiO}_2$  nanomaterials was calculated using Tauc plots, where the intercept of the tangent to the plot  $(\alpha h\nu)^2$  versus  $h\nu$  gives a good estimation of the direct bandgap for a semiconductor. The optical absorbance coefficient of a semiconductor for direct transition is given by the equation

$$\alpha = A \frac{(h\nu - E_g)^n}{h\nu} \quad (2)$$

where  $h\nu$  = photon energy,  $\alpha$  = absorbance coefficient,  $E_g$  = bandgap energy,  $A$  = constant and the exponent ' $n$ ' depends on the type of transition and it may have values of 1/2, 2, 3/2 and 3, corresponding to the allowed direct, allowed indirect, forbidden direct and forbidden indirect transitions, respectively. As shown in the Figure 4b, undoped  $\text{TiO}_2$ , 0.15, 0.3, 0.45 and 0.6 mol% Ru-doped  $\text{TiO}_2$  nanomaterials have bandgap values of 3.16, 3.12, 3.05, 3.02 and 2.98 eV, respectively (straight-line intercept to the energy axis). The reduction in bandgap can be attributed to the insertion of Ru into the  $\text{TiO}_2$  lattice. Since the lower edge of the CB is made up of  $\text{Ti}^{4+}$  3d bands [15], the substitution of  $\text{Ti}^{4+}$  with the Ru cation might have affected the CB structure. A similar observation has been reported by Wang et al., Lu et al. and Ismael et al. [29,33,41].

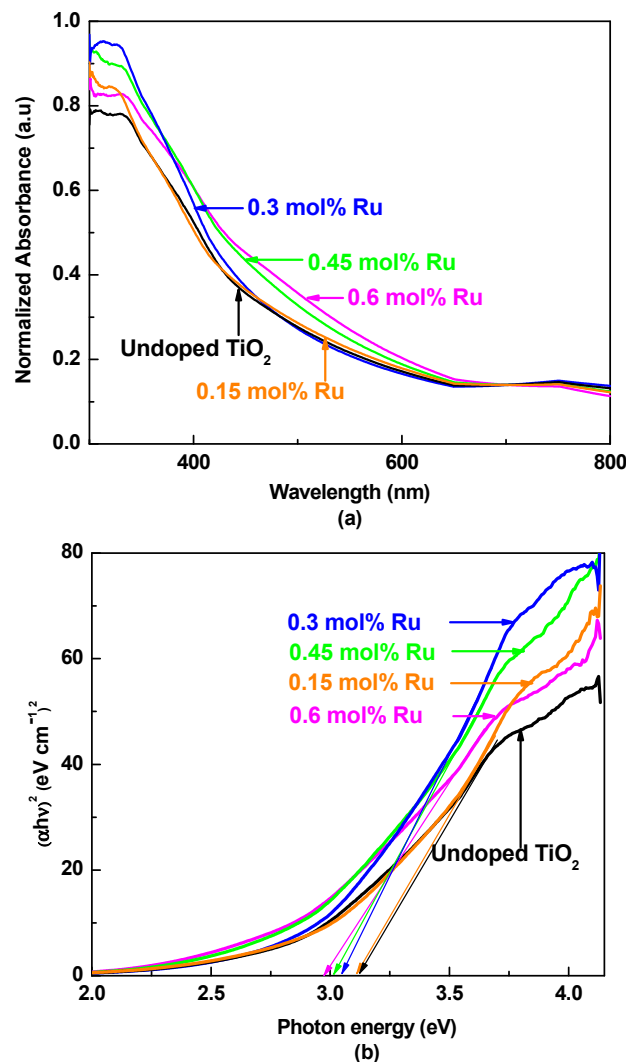


**Figure 4.** (a) UV–visible absorption spectra of undoped  $\text{TiO}_2$ , 0.15, 0.3, 0.45 and 0.6 mol% Ru-doped  $\text{TiO}_2$  nanomaterials; (b) Plot of  $(\alpha h\nu)^2$  versus Photon energy for undoped  $\text{TiO}_2$ , 0.15, 0.3, 0.45 and 0.6 mol% Ru-doped  $\text{TiO}_2$  nanomaterials.

### 3.3. Energy-Dispersive X-ray Spectroscopy

Figure 5 illustrates the elemental analysis of the undoped and Ru-doped TiO<sub>2</sub> samples, studied using energy-dispersive X-ray spectroscopy in the binding energy region of 0.0–20.0 KeV and the results are summarized in Table 1, which reveals the existence of Ti, O and Ru elements in Ru-doped TiO<sub>2</sub>.

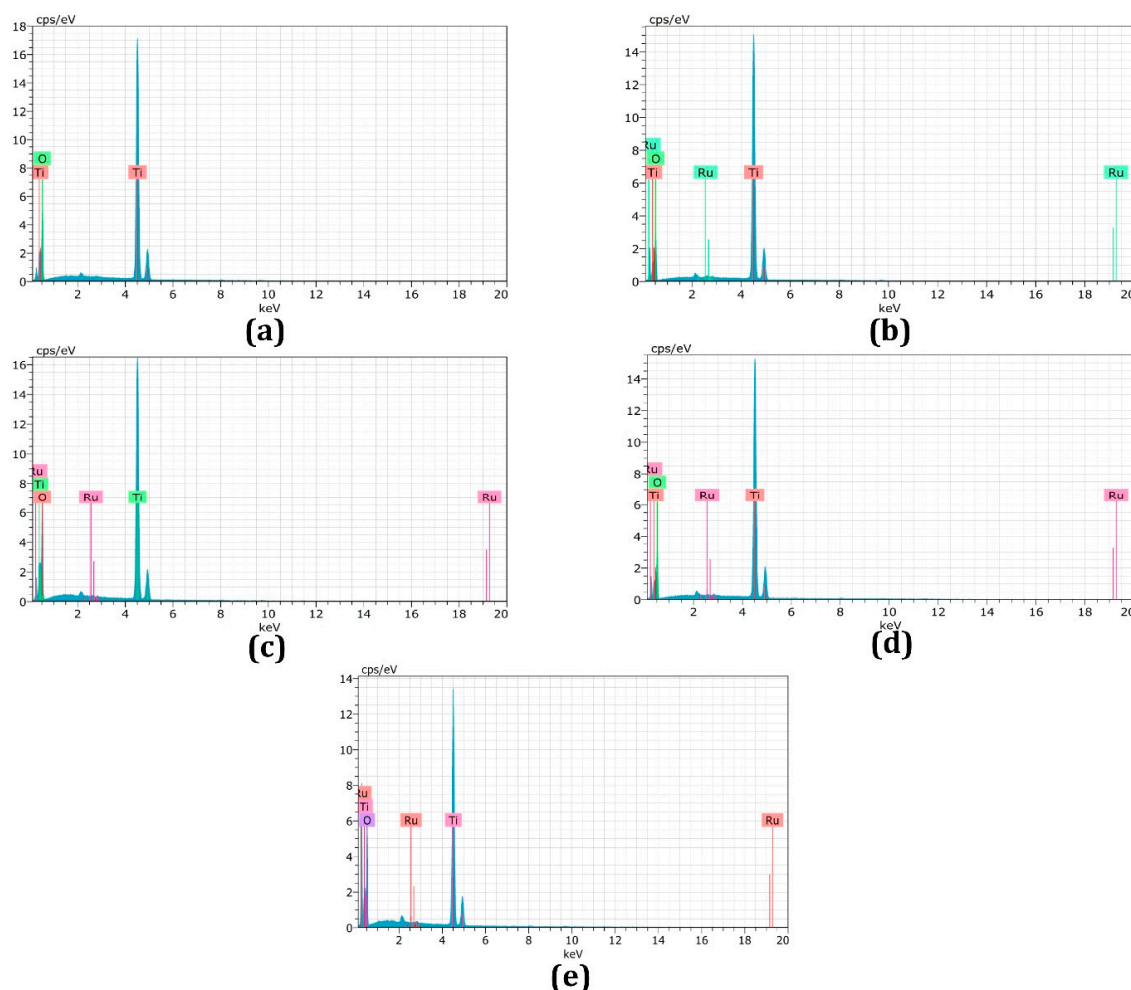


**Figure 5.** (a–e) EDX spectra of undoped and 0.15, 0.3, 0.45, 0.6 Ru-doped TiO<sub>2</sub> nanomaterials in the binding energy region from 0.0 to 20.0 KeV.

**Table 1.** Atomic percentage of Ru-doped TiO<sub>2</sub> in terms of energy-dispersive X-ray (EDX) investigation.

Samples	EDX Result-Ru at. %
Undoped TiO <sub>2</sub> (a)	0
0.15 mol% Ru (b)	0.10
0.30 mol% Ru (c)	0.25
0.45 mol% Ru (d)	0.46
0.60 mol% Ru (e)	0.75

### 3.4. J–V Characteristics

Figure 6a represents the J–V characteristics of DSSCs (in each type four devices were made and readings of the champion cells have been reported) made of photoanodes containing TiO<sub>2</sub> electrodes doped with different mol% of Ru and its control under simulated irradiation intensity of 100 mWcm<sup>−2</sup> with AM 1.5 filter. The corresponding photovoltaic parameters such as the short circuit current density

( $J_{SC}$ ), open-circuit photovoltage ( $V_{OC}$ ), fill factor (FF) and power conversion efficiency ( $\eta$ ) of these cells with Ru-doped  $TiO_2$  electrodes and undoped  $TiO_2$  electrode are summarized in Table 2. Moreover, Figure 6b indicates the influence of different Ru mol% dopant on  $J_{SC}$  and  $\eta$ . Ru-doping produces little improvement in  $V_{OC}$  and FF. The control cell showed  $V_{OC}$  of 0.66 V, which slightly increased to 0.69 V when 0.3 mol% Ru was doped. When the mol% of Ru dopant increases,  $J_{SC}$  shows a slight increase from 12.9 to 14.42  $mAcm^{-2}$  up to 0.15 mol% Ru and then it attains a maximum of 14.73  $mA/cm^2$  for 0.3 mol% Ru, subsequently, the  $J_{SC}$  values show a downward trend with further increase in Ru mol%. A similar trend was reflected in the  $\eta$  versus Ru mol% plot. The overall efficiency of the cell is mainly influenced by  $J_{SC}$ . Similar observations have been reported by So and co-workers (2012) in DSSCs with Ru-doped  $TiO_2$  nanotubes [32]. In our study, the cell fabricated with 0.3 mol% Ru-doped  $TiO_2$  electrode showed the best  $\eta$  of 7% which is over 20% enhancement relative to undoped  $TiO_2$  based DSSC ( $\eta = 5.78\%$ ).

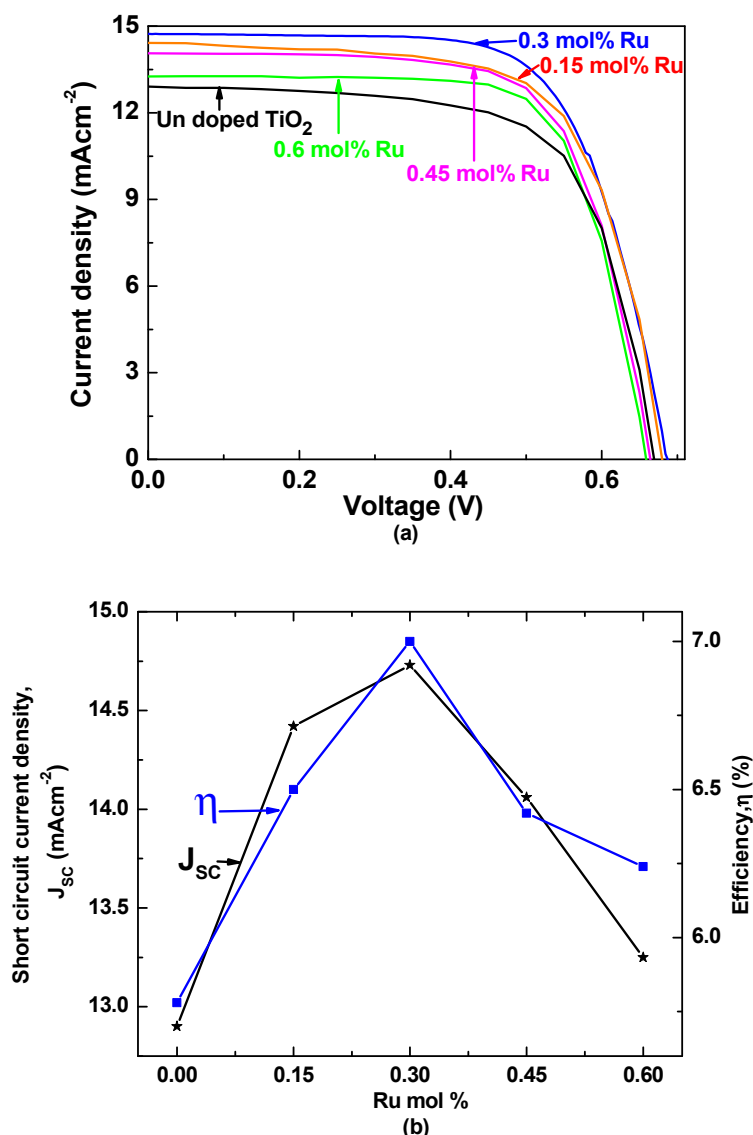


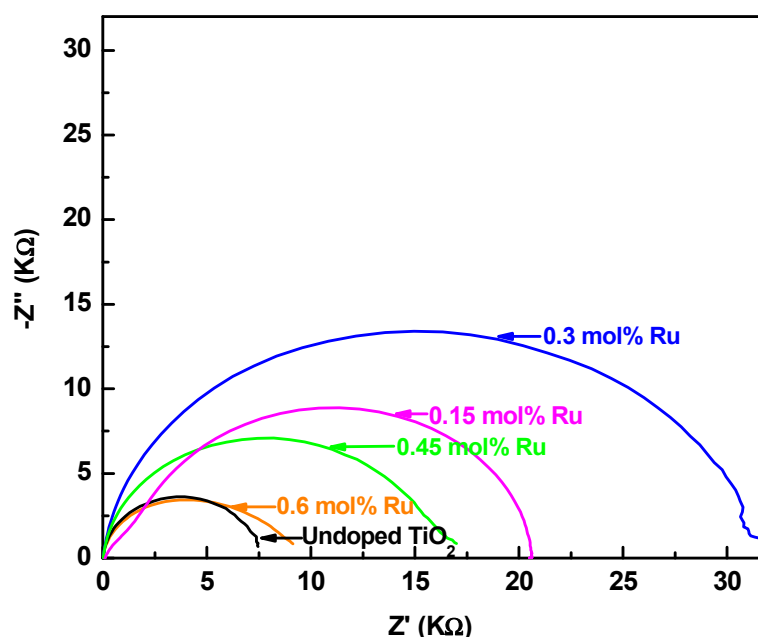
**Figure 6.** (a) Current–voltage (J–V) characteristic curves of the dye-sensitized solar cells (DSSCs) assembled with 0.15, 0.3, 0.45 and 0.6 mol% Ru-doped  $TiO_2$  photoanodes and its control undoped  $TiO_2$  photoanode under simulated irradiation of intensity  $100\text{ mWcm}^{-2}$  with AM 1.5 filter; (b) variations in  $J_{sc}$  and  $\eta$  with different mol% Ru dopants).

**Table 2.** Current-voltage (J–V) characteristics of the DSSCs assembled with different mol% Ru-doped P25-TiO<sub>2</sub> photoanodes and its control P25-TiO<sub>2</sub> photoanodes.

mol% of Ru in TiO <sub>2</sub>	J <sub>SC</sub> (mA/cm <sup>2</sup> )	V <sub>OC</sub> (V)	FF	η (%)
0.6	13.25	0.66	0.70	6.24
0.45	14.06	0.66	0.68	6.42
0.3	14.73	0.69	0.68	7.00
0.15	14.42	0.67	0.67	6.50
0	12.90	0.66	0.66	5.78

### 3.5. Electrochemical Impedance Spectroscopy

The interfacial charge transport phenomena of the DSSCs can be studied using electrochemical impedance spectroscopy (EIS). Figure 7 shows the Nyquist plots of the electrochemical impedance spectra of DSSCs based on the control and 0.15, 0.3, 0.45 and 0.6 mol% Ru-doped TiO<sub>2</sub> photoanodes, which were measured at frequencies from 10<sup>-2</sup> to 10<sup>6</sup> Hz in the dark, with a bias applied voltage of 10 mV [24]. The small semicircle in the high-frequency range corresponds to the charge transfer resistance (R<sub>1</sub>), which is related to the charge transfer at the interface of the electrolyte/Pt counter electrode and FTO/TiO<sub>2</sub> interface. A larger semicircle in the low frequency region is mainly related to the charge recombination resistance (R<sub>2</sub>) across the TiO<sub>2</sub>/electrolyte interface with a partial contribution from electron transport and accumulation in TiO<sub>2</sub> photoanode [44]. R<sub>1</sub> and R<sub>2</sub> values can be estimated from the diameter of the semicircles and resistance related to electron recombination (R<sub>2</sub>) increases with Ru-doping up to 0.3 mol% and then it starts to decrease with the increase in concentration of Ru. The higher values of resistance related to electron recombination indicate reduced electron recombination in Ru-doped electrodes [45]. This is the reason for the higher J<sub>sc</sub> values for the Ru-doped devices in the J–V measurement [32] even though increased recombination resistance and reduced recombination rate improve the Voc of the Ru-doped devices, this can also be attributed to the reduction in the bandgap as well [15]. A similar observation was reported by Wang et al. in perovskite solar cells [29] and also Ismael et al. (2019) reported that Ru-doping could facilitate the separation and migration of photogenerated electron–hole pairs [41].

**Figure 7.** Nyquist plot of DSSCs with 0.15, 0.3, 0.45, 0.6 mol% Ru-doped TiO<sub>2</sub> photoanodes and the control cell in dark.

#### 4. Conclusions

In the present study, Ru-doped TiO<sub>2</sub> electrodes were fabricated by treating TiO<sub>2</sub> with RuCl<sub>3</sub>·xH<sub>2</sub>O and by systematically varying the Ru content from 0.15% to 0.6%. The XRD pattern of Ru-doped TiO<sub>2</sub> nanomaterial confirms the presence of mixed anatase and rutile phases of TiO<sub>2</sub>. Optical absorption spectra of pure TiO<sub>2</sub> and Ru-doped TiO<sub>2</sub> reveal a slight red shift in the absorption spectrum upon Ru-doping. Among the DSSCs fabricated, the cell with 0.3 mol% Ru-doped TiO<sub>2</sub> electrode exhibited an optimum efficiency which is over 20% enhancement when compared to the control cell under stimulated AM 1.5 filter (100 mWcm<sup>-2</sup>, 1 sun). The EIS analysis of the cells confirms that charge recombination resistance is significantly increased upon Ru-doping that effectively suppresses the charge recombination rate, which results in better electron transport in the cell.

**Author Contributions:** Conceptualization, M.S., P.R. and D.V.; methodology, T.R., M.S. and P.R.; formal analysis, T.R., P.R. and D.V.; resources, D.V., M.N. and P.R.; data curation, T.R., M.S., P.R. and D.V.; writing—original draft preparation, T.R.; writing—review and editing, M.S., P.R., M.N. and D.V.; supervision, M.S., P.R. and D.V.; project administration, D.V. and P.R.; funding acquisition, D.V. and P.R. All authors have read and agreed to the published version of the manuscript.

**Funding:** This research was funded by Capacity Building and Establishment of a Research Consortium (CBERC) project, grant number LKA-3182-HRNCET and Higher Education and Research collaboration on Nanomaterials for Clean Energy Technologies (HRNCET) project, Grant number NORPART/2016/10237.

**Acknowledgments:** P. Balraju, Coimbatore Institute of Technology, India for SEM measurement, K. Vignarooban, University of Jaffna, Sri Lanka for EIS measurement, Akila Yuvapragasam, PSG Institute of Technology and Applied Research, India for the critical reading of the manuscript and P.R. acknowledge National Research Council, Sri Lanka for Metrohm Autolab Potentiostat/galvanostat.

**Conflicts of Interest:** The authors declare no conflict of interest. The funders had no role in the design of the study; in the collection, analyses or interpretation of data; in the writing of the manuscript, or in the decision to publish the results.

#### References

1. Kay, A.; Grätzel, M. Dye-sensitized core-shell nanocrystals: Improved efficiency of mesoporous tin oxide electrodes coated with a thin layer of an insulating oxide. *Chem. Mater.* **2002**, *14*, 2930–2935. [[CrossRef](#)]
2. Burnside, S.; Moser, J.-E.; Brooks, K.; Grätzel, M.; Cahen, D. Nanocrystalline mesoporous strontium titanate as photoelectrode material for photosensitized solar devices: Increasing photovoltage through flatband potential engineering. *J. Phys. Chem. B* **1999**, *103*, 9328–9332. [[CrossRef](#)]
3. Sayama, K.; Sugihara, H.; Arakawa, H. Photoelectrochemical properties of a porous Nb<sub>2</sub>O<sub>5</sub> electrode sensitized by a ruthenium dye. *Chem. Mater.* **1998**, *10*, 3825–3832. [[CrossRef](#)]
4. Saito, M.; Fujihara, S. Large photocurrent generation in dye-sensitized ZnO solar cells. *Energy Environ. Sci.* **2008**, *1*, 280–283. [[CrossRef](#)]
5. O'Regan, B.; Grätzel, M. A low-cost, high-efficiency solar cell based on dye-sensitized colloidal TiO<sub>2</sub> films. *Nature* **1991**, *353*, 737–740. [[CrossRef](#)]
6. Gokilamani, N.; Muthukumarasamy, N.; Thambidurai, M.; Ranjitha, A.; Velauthapillai, D. Utilization of natural anthocyanin pigments as photosensitizers for dye-sensitized solar cells. *J. Sol-Gel Sci. Technol.* **2013**, *66*, 212–219. [[CrossRef](#)]
7. Prabavathy, N.; Balasundaraprabhu, R.; Balaji, G.; Malikaramage, A.; Prasanna, S.; Sivakumaran, K.; Kumara, G.; Rajapakse, R.; Velauthapillai, D. Investigations on the photo catalytic activity of calcium doped TiO<sub>2</sub> photo electrode for enhanced efficiency of anthocyanins based dye sensitized solar cells. *J. Photochem. Photobiol. A Chem.* **2019**, *377*, 43–57. [[CrossRef](#)]
8. Prabavathy, N.; Shalini, S.; Balasundaraprabhu, R.; Velauthapillai, D.; Prasanna, S.; Muthukumarasamy, N. Enhancement in the photostability of natural dyes for dye-sensitized solar cell (DSSC) applications: A review. *Int. J. Energy Res.* **2017**, *41*, 1372–1396. [[CrossRef](#)]
9. Senthil, T.; Muthukumarasamy, N.; Velauthapillai, D.; Agilan, S.; Thambidurai, M.; Balasundaraprabhu, R. Natural dye (cyanidin 3-O-glucoside) sensitized nanocrystalline TiO<sub>2</sub> solar cell fabricated using liquid electrolyte/quasi-solid-state polymer electrolyte. *Renew. Energy* **2011**, *36*, 2484–2488. [[CrossRef](#)]

10. Tennakone, K.; Hewaparakkrama, K.; Dewasurendra, M.; Jayatissa, A.; Weerasena, L. Dye-sensitized solid-state photovoltaic cells. *Semicond. Sci. Technol.* **1988**, *3*, 382. [[CrossRef](#)]
11. Memarian, N.; Concina, I.; Braga, A.; Rozati, S.M.; Vomiero, A.; Sberveglieri, G. Hierarchically assembled ZnO nanocrystallites for high-efficiency dye-sensitized solar cells. *Angew. Chem. Int. Ed.* **2011**, *50*, 12321–12325. [[CrossRef](#)]
12. Nazeeruddin, M.K.; Baranoff, E.; Grätzel, M. Dye-sensitized solar cells: A brief overview. *Sol. Energy* **2011**, *85*, 1172–1178. [[CrossRef](#)]
13. Roose, B.; Pathak, S.; Steiner, U. Doping of TiO<sub>2</sub> for sensitized solar cells. *Chem. Soc. Rev.* **2015**, *44*, 8326–8349. [[CrossRef](#)]
14. Tanyi, A.R.; Rafieh, A.I.; Ekaneyaka, P.; Tan, A.L.; Young, D.J.; Zheng, Z.; Chellappan, V.; Subramanian, G.S.; Chandrakanthi, R. Enhanced efficiency of dye-sensitized solar cells based on Mg and La co-doped TiO<sub>2</sub> photoanodes. *Electrochim. Acta* **2015**, *178*, 240–248. [[CrossRef](#)]
15. Mehnane, H.F.; Wang, C.; Kondamareddy, K.K.; Yu, W.; Sun, W.; Liu, H.; Bai, S.; Liu, W.; Guo, S.; Zhao, X.-Z. Hydrothermal synthesis of TiO<sub>2</sub> nanoparticles doped with trace amounts of strontium, and their application as working electrodes for dye sensitized solar cells: Tunable electrical properties & enhanced photo-conversion performance. *RSC Adv.* **2017**, *7*, 2358–2364.
16. Yang, S.; Guo, S.; Xu, D.; Xue, H.; Kou, H.; Wang, J.; Zhu, G. Improved efficiency of dye-sensitized solar cells applied with F-doped TiO<sub>2</sub> electrodes. *J. Fluor. Chem.* **2013**, *150*, 78–84. [[CrossRef](#)]
17. Sun, Q.; Zhang, J.; Wang, P.; Zheng, J.; Zhang, X.; Cui, Y.; Feng, J.; Zhu, Y. Sulfur-doped TiO<sub>2</sub> nanocrystalline photoanodes for dye-sensitized solar cells. *J. Renew. Sustain. Energy* **2012**, *4*, 023104. [[CrossRef](#)]
18. Xing, G.; Zhang, Z.; Qi, S.; Zhou, G.; Zhang, K.; Cui, Z.; Feng, Y.; Shan, Z.; Meng, S. Effect of cerium ion modifications on the photoelectrochemical properties of TiO<sub>2</sub>-based dye-sensitized solar cells. *Opt. Mater.* **2018**, *75*, 102–108. [[CrossRef](#)]
19. Sakthivel, T.; Kumar, K.A.; Ramanathan, R.; Senthilselvan, J.; Jagannathan, K. Silver doped TiO<sub>2</sub> nano crystallites for dye-sensitized solar cell (DSSC) applications. *Mater. Res. Express* **2017**, *4*, 126310. [[CrossRef](#)]
20. Ranjitha, A.; Muthukumarasamy, N.; Thambidurai, M.; Velauthapillai, D. Enhanced photovoltaic performance of quantum dot sensitized solar cells with Ag-doped TiO<sub>2</sub> nanocrystalline thin films. *J. Mater. Sci. Mater. Electron.* **2014**, *25*, 2724–2729. [[CrossRef](#)]
21. Yacoubi, B.; Samet, L.; Bennaceur, J.; Lamouchi, A.; Chtourou, R. Properties of transition metal doped-titania electrodes: Impact on efficiency of amorphous and nanocrystalline dye-sensitized solar cells. *Mater. Sci. Semicond. Process.* **2015**, *30*, 361–367. [[CrossRef](#)]
22. Jin, E.M.; Jeong, S.M.; Kang, H.-C.; Gu, H.-B. Photovoltaic effect of metal-doped TiO<sub>2</sub> nanoparticles for dye-sensitized solar cells. *ECS J. Solid State Sci. Technol.* **2016**, *5*, Q109–Q114. [[CrossRef](#)]
23. Asemi, M.; Maleki, S.; Ghanaatshoar, M. Cr-doped TiO<sub>2</sub>-based dye-sensitized solar cells with Cr-doped TiO<sub>2</sub> blocking layer. *J. Sol-Gel Sci. Technol.* **2017**, *81*, 645–651. [[CrossRef](#)]
24. Lü, X.; Mou, X.; Wu, J.; Zhang, D.; Zhang, L.; Huang, F.; Xu, F.; Huang, S. Improved-performance dye-sensitized solar cells using Nb-doped TiO<sub>2</sub> electrodes: Efficient electron injection and transfer. *Adv. Funct. Mater.* **2010**, *20*, 509–515. [[CrossRef](#)]
25. Tong, Z.; Peng, T.; Sun, W.; Liu, W.; Guo, S.; Zhao, X.-Z. Introducing an intermediate band into dye-sensitized solar cells by W<sup>6+</sup> doping into TiO<sub>2</sub> nanocrystalline photoanodes. *J. Phys. Chem. C* **2014**, *118*, 16892–16895. [[CrossRef](#)]
26. Wijayarathna, T.; Aponso, G.; Ariyasinghe, Y.; Premalal, E.; Kumara, G.; Tennakone, K. A high efficiency indoline-sensitized solar cell based on a nanocrystalline TiO<sub>2</sub> surface doped with copper. *Nanotechnology* **2008**, *19*, 485703. [[CrossRef](#)]
27. Qu, X.; Hou, Y.; Liu, M.; Shi, L.; Zhang, M.; Song, H.; Du, F. Yttrium doped TiO<sub>2</sub> porous film photoanode for dye-sensitized solar cells with enhanced photovoltaic performance. *Results Phys.* **2016**, *6*, 1051–1058. [[CrossRef](#)]
28. Latini, A.; Cavallo, C.; Aldibaja, F.K.; Gozzi, D.; Carta, D.; Corrias, A.; Lazzarini, L.; Salviati, G. Efficiency improvement of DSSC photoanode by scandium doping of mesoporous titania beads. *J. Phys. Chem. C* **2013**, *117*, 25276–25289. [[CrossRef](#)]
29. Wang, S.; Liu, B.; Zhu, Y.; Ma, Z.; Miao, X.; Ma, R.; Wang, C.-Y. Enhanced performance of TiO<sub>2</sub>-based perovskite solar cells with Ru-doped TiO<sub>2</sub> electron transport layer. *Sol. Energy* **2018**, *169*, 335–342. [[CrossRef](#)]

30. Houšková, V.; Štengl, V.; Bakardjieva, S.; Murafa, N.; Tyrpekl, V. Efficient gas phase photodecomposition of acetone by Ru-doped Titania. *Appl. Catal. B Environ.* **2009**, *89*, 613–619. [[CrossRef](#)]
31. Kong, D.; Jin, X.; Sun, W.; Du, J.; Tong, J.; Chen, C.; Yang, X.; Cheng, Y.; Li, Q. Ruthenium cation substitutional doping for efficient charge carrier transfer in organic/inorganic hybrid solar cells. *J. Power Sources* **2015**, *274*, 701–708. [[CrossRef](#)]
32. So, S.; Lee, K.; Schmuki, P. Ru-doped TiO<sub>2</sub> nanotubes: Improved performance in dye-sensitized solar cells. *Phys. Status Solidi (RRL) Rapid Res. Lett.* **2012**, *6*, 169–171. [[CrossRef](#)]
33. Lu, W.-H.; Chou, C.-S.; Chen, C.-Y.; Wu, P. Micro-and electronic structure optimization of Ru-doped TiO<sub>2</sub> electrodes for efficient dye-sensitized solar cells. *Sol. Energy* **2016**, *139*, 318–327. [[CrossRef](#)]
34. Ohno, T.; Tanigawa, F.; Fujihara, K.; Izumi, S.; Matsumura, M. Photocatalytic oxidation of water by visible light using ruthenium-doped titanium dioxide powder. *J. Photochem. Photobiol. A Chem.* **1999**, *127*, 107–110. [[CrossRef](#)]
35. Senthilnathan, M.; Ho, D.; Vigneswaran, S.; Ngo, H.; Shon, H. Visible light responsive ruthenium-doped titanium dioxide for the removal of metsulfuron-methyl herbicide in aqueous phase. *Sep. Purif. Technol.* **2010**, *75*, 415–419. [[CrossRef](#)]
36. Upadhyay, P.; Srivastava, V. Synthesis of ruthenium metal doped titanium dioxide nanoparticles for CO<sub>2</sub> hydrogenation. *AIP Conf. Proc.* **2016**, *1724*, 020074.
37. Lim, S.P.; Pandikumar, A.; Lim, H.N.; Ramaraj, R.; Huang, N.M. Boosting photovoltaic performance of dye-sensitized solar cells using silver nanoparticle-decorated N, S-Co-doped-TiO<sub>2</sub> photoanode. *Sci. Rep.* **2015**, *5*, 11922. [[CrossRef](#)]
38. Thambidurai, M.; Foo, S.; Salim, K.M.; Harikesh, P.; Bruno, A.; Jamaludin, N.F.; Lie, S.; Mathews, N.; Dang, C. Improved photovoltaic performance of triple-cation mixed-halide perovskite solar cells with binary trivalent metals incorporated into the titanium dioxide electron transport layer. *J. Mater. Chem. C* **2019**, *7*, 5028–5036. [[CrossRef](#)]
39. Loheeswaran, S.; Thanihaichelvan, M.; Ravirajan, P.; Nelson, J. Controlling recombination kinetics of hybrid poly-3-hexylthiophene (P3HT)/titanium dioxide solar cells by self-assembled monolayers. *J. Mater. Sci. Mater. Electron.* **2017**, *28*, 4732–4737. [[CrossRef](#)]
40. Thanihaichelvan, M.; Sockiah, K.; Balashangar, K.; Ravirajan, P. Cadmium sulfide interface layer for improving the performance of titanium dioxide/poly (3-hexylthiophene) solar cells by extending the spectral response. *J. Mater. Sci. Mater. Electron.* **2015**, *26*, 3558–3563. [[CrossRef](#)]
41. Ismael, M. High effective ruthenium-doped TiO<sub>2</sub> nanoparticles photocatalyst for visible-light-driven photocatalytic hydrogen production. *New J. Chem.* **2019**, *43*, 9596–9605. [[CrossRef](#)]
42. Elezović, N.; Babić, B.; Radmilovic, V.; Vračar, L.M.; Krstajić, N. Novel Pt catalyst on ruthenium doped TiO<sub>2</sub> support for oxygen reduction reaction. *Appl. Catal. B Environ.* **2013**, *140*, 206–212. [[CrossRef](#)]
43. Madurai, V.; Natarajan, M.; Santhanam, A.; Asokan, V.; Velauthapillai, D. Size controlled synthesis of TiO<sub>2</sub> nanoparticles by modified solvothermal method towards effective photocatalytic and photovoltaic applications. *Mater. Res. Bull.* **2018**, *97*, 351–360.
44. Thambidurai, M.; Shini, F.; Harikesh, P.; Mathews, N.; Dang, C. Highly stable and efficient planar perovskite solar cells using ternary metal oxide electron transport layers. *J. Power Sources* **2020**, *448*, 227362. [[CrossRef](#)]
45. Shini, F.; Thambidurai, M.; Harikesh, P.; Mathews, N.; Huang, Y.; Dang, C. Heterogeneous electron transporting layer for reproducible, efficient and stable planar perovskite solar cells. *J. Power Sources* **2019**, *437*, 226907. [[CrossRef](#)]

